Shahid Chamran University of Ahvaz

Iranian Association of Electrical and Electronics Engineers

Journal of Applied Research in Electrical Engineering

E-ISSN: 2783-2864
P-ISSN: 2717-414X
Homepage: https://jaree.scu.ac.ir/

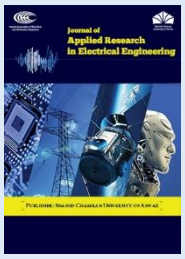

Research Article

Influence of Gas Insulated Switchgear Configuration Components on UHF PD Signals

Reza Rostaminia*, Mehdi Vakilian, and Keyvan Firouzi

Electrical Engineering Department and Centre of Excellence in Power System Management and Control,

Sharif University of Technology, Tehran 1458889694, Iran

** Corresponding Author: Reza_rostaminia@ee.sharif.edu*

Abstract: Partial Discharge (PD) measurement is one of the main methods for condition monitoring of Gas Insulated Switchgears (GIS). Internal Ultra High Frequency (UHF) sensors can be applied for capturing PD propagated electromagnetic signals within the GIS. PD sensor placement inside the GIS is one of the main challenges for designing an online PD measuring system. For this aim, the impacts of different GIS components on propagated PD electromagnetic waves should be studied. In this paper, different PD sensor position angles (with respect to PD sensor) are used to investigate their sensitivity to measuring PD electromagnetic waves. Two distinguishable parameters from the calculated PD electromagnetic waves, the first rated electric field and the signal's power over the two frequency ranges (0.3-2 GHz and 0.3-3 GHz) are used to analyze and quantify the calculation results. The impacts of different enclosure diameters, different types of spacers, and various disconnector contact gap distances (under different voltage levels) on this wave propagation are studied. Additionally, the two standard GIS busbar profiles, named L-shape and T-shape, are discussed in this paper. The results show that the attenuation degree of the measured PD EM waves is strongly influenced by the busbar dimensions and the configuration of its components. The GIS busbar designer can employ these results to select the proper PD sensors and their installation locations.

Keywords: Gas insulated switchgear, partial discharge, ultra-high frequency measurements, electric field and electromagnetic wave.

Article history
Received 13 December 2021; Revised 21 December 2021; Accepted 23 December 2021; Published online 8 March 2022.

How to cite this article
R. Rostaminia, M. Vakilian, and K. Firouzi, "Influence of gas insulated switchgear configuration components on UHF PD signals," *J. Appl. Res. Electr. Eng.*, vol. 1, no. 2, pp. 139-148, 2022. DOI:10.22055/jaree.2021.39436.1039

Check for updates

1. INTRODUCTION

Ultra-High Frequency (UHF) Partial Discharge (PD) measurement is one of the most proper approaches to detecting defects within gas-insulated switchgear (GIS) in the early stages. Many studies have used this method in recent years [1-4]. In general, these research studies can be classified into the design and manufacturing of various UHF couplers and measuring systems, the PD location within GIS, and the identification of PD defect types and the degree of PD fault progress within the GIS.

One of the main challenges in using the UHF PD measurement technique in high voltage equipment is selecting a criterion for severity analysis of the measured PD. CIGRE working group D1.25 has proposed two steps for sensitivity verification of UHF PD measurement in GIS [5]. The CIGRE report aims to compare the measured PD magnitude from the UHF method with the conventional IEC60270 method. Many items can influence the PD signal measured with the UHF method. [7] proposed a hybrid method in which UHF PD detection is used to detect the PD discharges (due to its higher sensitivity), and IEC 60270 measure is used to determine its severity. These items can be summarized as the type of defects, the location of defects in GIS enclosure, propagation parameters like reflection, refraction, attenuation, the PD sensor position within GIS enclosure which can result in various signal transmission paths based on the PD defect position, the type of sensor employed and its transfer function, and finally, the characteristics of other measurement paths from sensors to a monitoring system. Although the CIGRE publication has proposed a preliminary recommendation for sensitivity verification of UHF PD couplers in GIS, new studies are under way to develop a major solution for UHF PD

measurement. To address this concern, first, the impacts of each part of GIS on the attenuation of electromagnetic PD signals should be determined. This could also help to determine the number of PD UHF couplers and their positions within each bay of GIS. The electromagnetic waves produced by a PD in GIS coaxial structure have three different modes, namely, TEM, TE, and TM [6]. The cutoff frequency of each electromagnetic mode depends on the dimension and constructional characteristics of the enclosure and the conductors in a GIS [8]. The EM mode components propagate through straight, L-shape, and T-shape structures of GIS, which are investigated in [9-12]. In other researches, the effects of different parts of a GIS on EM wave propagation have been investigated. In [13], the effect of two kinds of spacers, bush type, and metal flange type is investigated on EM PD wave propagation within GIS. In [14], the electromagnetic wave propagation within the GIS enclosure is examined, and the effects of the insulated gas barrier on the attenuation of EM waves have been analyzed. The Finite Difference Time Domain (FDTD) method has been applied by the authors to simulate the PD electromagnetic wave behavior in a GIS straight configuration. Also, in [15], the authors have analyzed the effects of gas barrier properties, including its thickness, dielectric constant, and the spacing between adjacent bolts and the profile of its flanges on the electromagnetic PD wave leakage. In [8, 16], the authors have explored the effects of main GIS conductor discontinuity (such as the disconnectors discontinuity) on PD EM waves detected by the UHF sensors. Also, in [17] some experiments have been carried out on 66 kV and 154 kV T-shape GIS structures to investigate the PD EM wave mode of propagation through the GIS coaxial structure. In [18], the L-branch structure of 66 kV GIS has been selected to examine the attenuation implemented into PD EM waves in the TEM and TE modes.

Although extensive research has already been carried out on the effects of different parameters on PD EM wave propagation within GIS, more studies are still required on optimum placements of PD UHF sensors when using different busbar arrangements and under various voltage levels. One of the main difficulties in the evaluation of the results of PD EM wave propagation within GIS is the differences that exist among the wave shapes and amplitudes of the PD discharge pulses captured in each PD occurrence. Meanwhile, many parameters may have an impact on the measured PD EM waves, and it is very difficult to explore the exact effect of each one of them on the captured PD EM waves originated from different PD sources. Hence, to solve these problems, in this paper, a simulation model of GIS is developed in CST Microwave Studio software to study the effects of different parameters on PD EM wave behavior while a standard wave shape of PD is applied to the model. Therefore, first, the position of the UHF sensors with respect to the PD source location is determined. Then, the impacts of different enclosure sizes are investigated under various rated voltage levels of GIS. The effects of different parameters of the spacer, such as its thickness and type (i.e., in the form of barrier or support insulator), are studied. Then, the effects of disconnecting contacts (such as circuit breakers or disconnector contacts with various gap distances under different voltage levels) are analyzed. Additionally, the L-shape and T-shape GIS and their structural impacts on the propagation of PD-based EM waves are investigated.

2. SIMULATION MODEL

2.1. Straight Structure

The CST Microwave Studio software is chosen to study PD-based EM wave propagation within the GIS model. At the first step, a straight GIS structure model is selected for the study. The impacts of the UHF sensor position with respect to the PD source position, the enclosure diameters, the spacer types, the contact thicknesses, the disconnector contact gap distance on the PD-related EM wave propagation (Fig. 1) are studied.

The length of the straight structure in this GIS sample is about 4.22 m. Its five compartments are considered to have a straight structure GIS model, while the length of each gas compartment, numbered 1 to 4, is 1 m, and the compartment number 5 is 20 cm long.

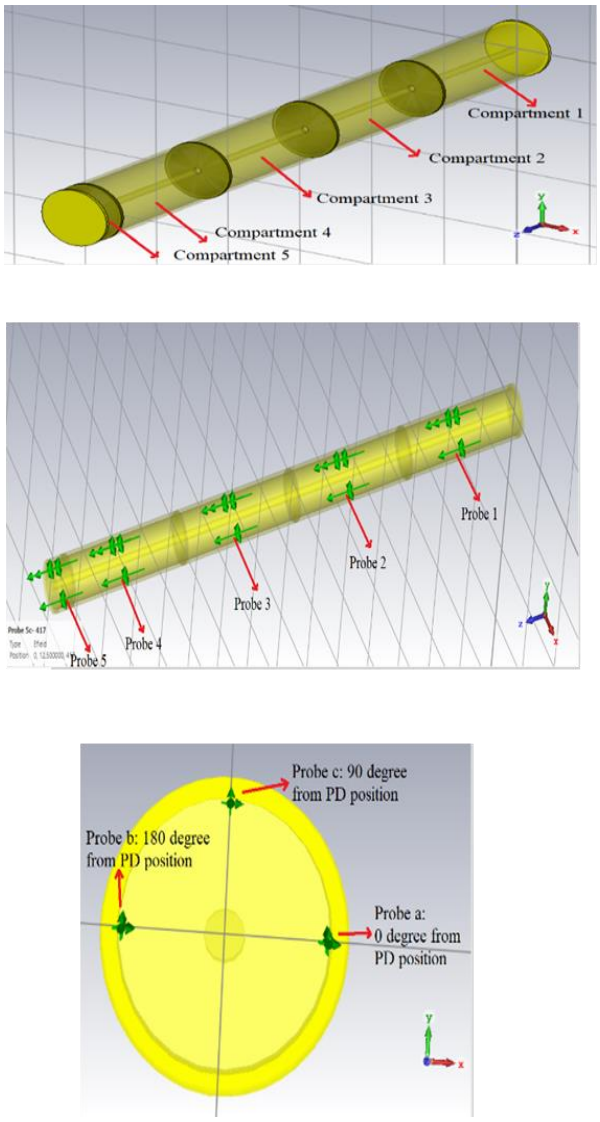

Fig. 1: Straight structure model of GIS in CST software.

The main conductor is made of aluminum. The material of the spacer insulator is epoxy resin with a thickness of 2 cm. At the two ends of the structure, two flanges with a thickness of 2 cm and the same diameter as the GIS enclosures are fitted. As it is shown in Fig. 1-c, three UHF PD probes (probe A, probe B, and probe C) are located at angles of 0°, 180°, and 90° versus the PD source (in GIS enclosure), respectively. Each probe is placed at the middle of the related compartment length while the PD source is located near the GIS main conductor along the probe-A in the middle of compartment 1.

In each compartment, there are three UHF probes located in the abovementioned direction angles with respect to the PD source. The PD current wave shape is a gaussian current pulse of 1 ns width and 15 mA amplitude representing 5 pc charge of PD (Fig. 2).

To study the difference between the effects of a barrier insulator and a support insulator on PD EM wave propagation, two types of support insulator, one with three holes and the other with four holes, are employed (Fig. 3).

Each hole has a diameter of 4 cm and is located in a symmetrical position with respect to the main conductor. To investigate the effects of the disconnector gap distance on PD-based EM wave propagation, a gap distance is implemented along the main conductor of compartment 2 (having a straight structure) (Fig.4). The length of its gap varies from 10 cm to 30 cm.

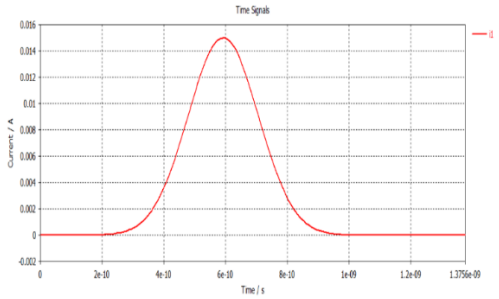

Fig. 2: The PD current gaussian wave shape.

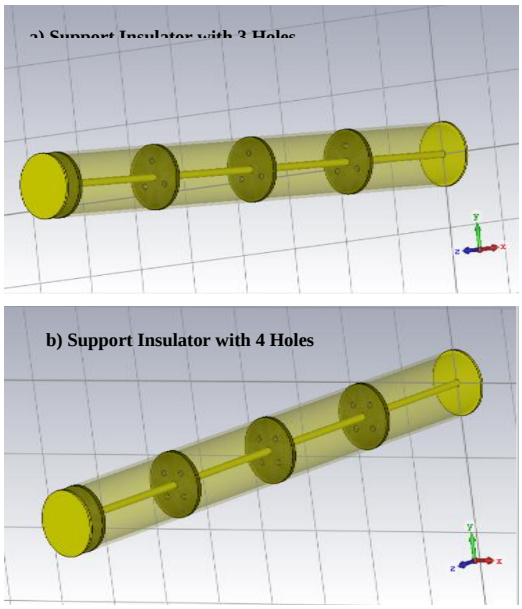

Fig. 3: Different types of support insulator as a spacer in the model, (a) with three holes, and (b) with four holes.

2.2. L-Shape Structure

Four gas compartments of the L-Shape structure are implemented to the GIS busbar in these studies. The diameter of the enclosure is 40 cm, and the length of each compartment is 1 m. In each compartment (chamber-bay), as in the straight structure model, three electric field probes are located at angles of 0°, 180°, and 90° with respect to the PD source position. The PD source is located in the middle of compartment 1, and the other dimensional parts of the model are the same as that of the straight model (Fig. 5).

2.3. T-Shape Structure

Six gas compartments are employed in the T-Shape structure model, and the length of each compartment is 1 m (Fig. 6). The PD source is placed in the middle of compartment 1. All of the other features of the model are the same as the straight structure model.

3. Simulation Results And Discussion

The simulation results obtained from electric field probes are shown in Fig. 7 in which the time-domain and frequency-domain PD calculated signal can be seen. The time differences of signals arrival, among the different installed probes (due to their distances from the PD) can be seen.

As it is evident, a lot of distortions exist in both the time-domain and frequency-domain captured signals. These distortions are due to reflections and refractions of PD EM waves within the enclosed metal enclosure of the GIS model. The first peak value of the signal in the time domain and the power of the signal in the frequency domain are selected as criteria to analyze and compare the different measurement results of PD signals under a specific condition. The UHF range of frequency is from 300 MHz to 3 GHz. However, in most commercial UHF antennas of PD measuring systems in GIS, the signal measurement frequency is limited to 2 GHz. Accordingly, two ranges of spectrum are chosen for signal power measurement in the frequency domain. Therefore, in each scenario, the following three parameters have been compared:

a- Emax: First peak of calculated electric field

b- PI: the power of the signal in frequency ranges between 300 MHz to 3 GHz.

c- PII: the power of the signal in frequency ranges between 300 MHz to 2 GHz.

As it is stated in the previous section, three probes with directions of 0°, 180°, and 90° with respect to the PD source position (probe A, probe B, and probe C, respectively) are considered. Hence, the differences between the results obtained from each one within the same compartments will be analyzed.

In Fig. 8, the electric fields calculated by these three probes are presented. The peak value of the electric field in each probe is per-united based on the value calculated by 'probe A' within compartment 1.

As it can be seen, the value of 'probe A' in compartment 1 is maximum due to the direct passage of the PD EM wave along with this probe. While 'probe B' and 'probe C' have values close to each other, which is about 0.3 with respect to the

'probe A' calculated value. Considering the values of 'Probe A' in compartments 1 to 5, it can be seen that except compartment 1, the other compartments have calculated values that are the same as each other. Also, this can be seen for 'probe B' and 'probe C' in compartments 1 to 5.

Fig. 9 depicts a comparison between the power of signals PI and PII in the two different frequency ranges. When comparing the values of these signals calculated by 'probe A', 'probe B', and 'probe C' in compartment 1, a significant reduction in signal power can be seen in 'probe A' versus the two other probes. However, the difference between powers calculated by 'probe A' and 'probe C' is more than the related difference of 'probe A' and 'probe B'. This is because of 90° direction angle of 'probe C' versus the PD source. The other important note in Fig. 9 is that the calculated values of the three probes in compartment 5 are increased versus the calculated values of the probes in the other compartments. This is due to the position of compartment 5, which is at the end of the employed GIS model. At the end of the model, the reflections of EM waves are intense, and these reflections contain a higher order of frequencies, which are more than 2 GHz. Therefore, the calculated values of probes in compartment 5, as shown in Fig. 9, are not higher than those in the other compartments. When comparing these against the results shown in Fig. 8, it can be seen that the calculated values of 'probe C' are significantly lower than the calculated values of 'probe A' and 'probe B'. Since in practice under the PD occurrence within the GIS, the position and direction angle of PD occurrence with respect to the PD sensor position within a compartment is unspecified, 'probe C' (the worst case) is selected for following the investigations.

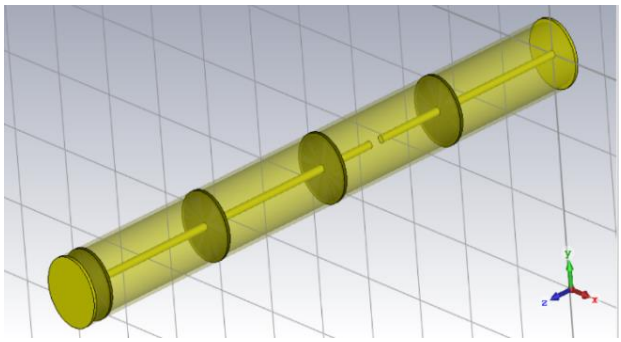

Fig. 4: The model of disconnector contacts in compartment 2 of the straight structure model.

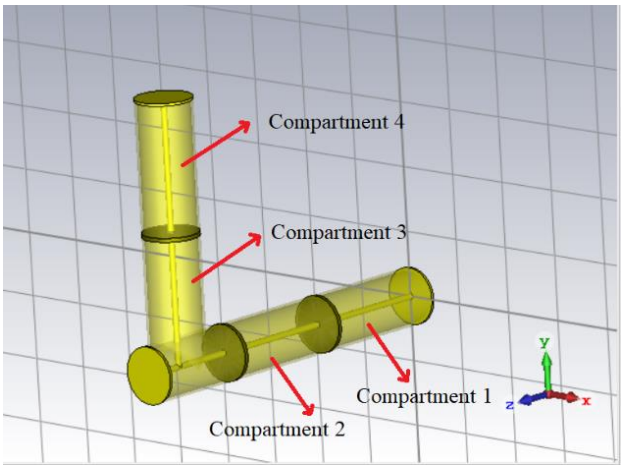

Fig. 5: The L-Shape structure of the model.

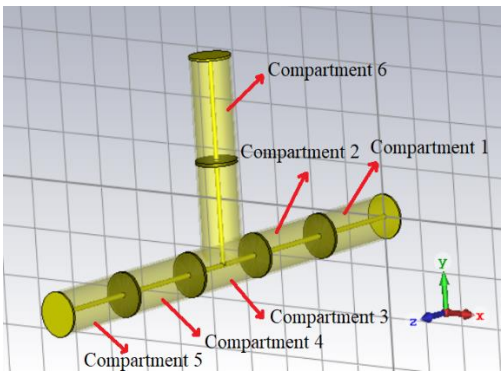

Fig. 6: The T-Shape structure of the model.

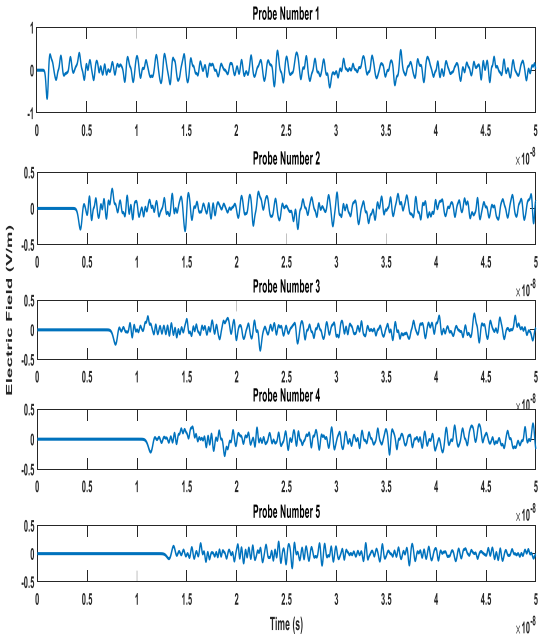

(a)

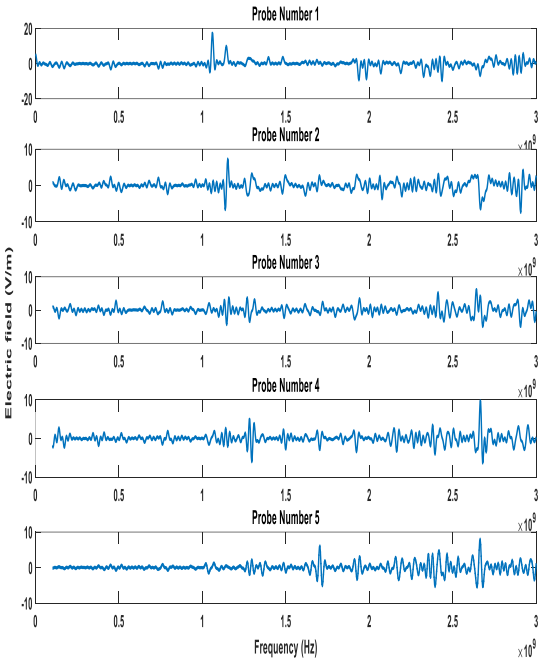

(b)

Fig. 7: Calculated PD EM wave with electric field probes: (a) Time-domain electric field, and (b) Frequency domain electric field.

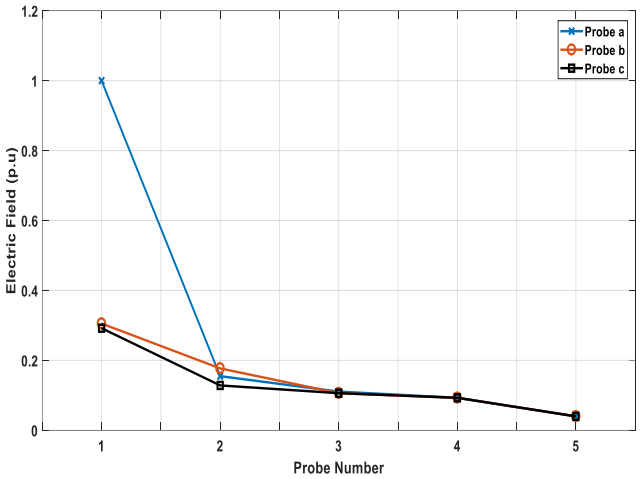

Fig. 8: Calculated electric field first peak in three sets of probe number 1.

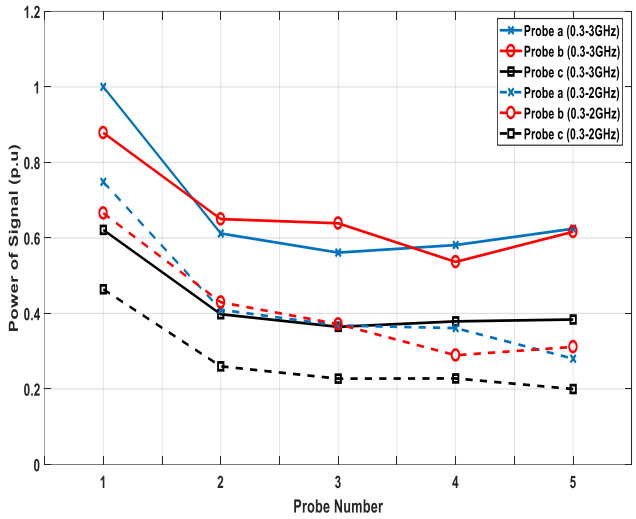

Fig. 9: The calculated signal power with frequency ranges 0.3-2 GHz and 0.3-3 GHz in three sets of probe number 1.

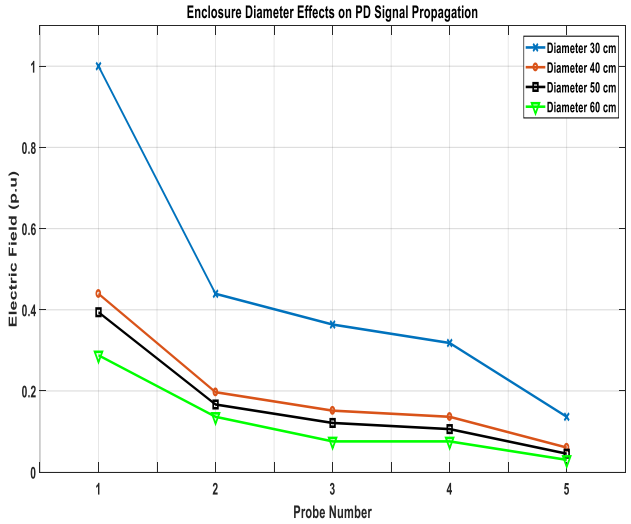

Fig. 10: The effects of different enclosure diameters on the first peak of the calculated electric field.

3.1. Effects of GIS Enclosure Diameters

Different voltage levels of GIS result in various sizes of enclosures. Multiple diameters of enclosures, i.e. 30 cm, 40 cm, 50 cm, and 60 cm, are selected to examine the effects of enclosure dimension on the propagation of PD EM wave. In this case, as the optimum design for a cylindrical GIS system, the diameter of the enclosure is considered 2.73 times the diameter of the main conductor [19]. Fig. 10 shows the electric fields calculated with 'probe C' in the five compartments (and for four diameters of the enclosure).

The electric field value for each probe is per-united based on the calculated value of 'probe C' in compartment 1 of 30 cm enclosure diameter.

As can be seen in Fig. 10, as the diameter of the enclosure increases, the calculated electric fields of each probe decrease. This is due to an increase in the distance of the PD source and the measurement probes; i.e., as the diameter of the enclosure increases, the length of the travel path for the PD-based EM wave signals will be enhanced. Although for each specific size of the enclosure, when the signal is passing compartment 1, the amplitude of the calculated PD signal decreases. There is a little difference between the calculated values located in an enclosure of 40 cm diameter with respect to a 60-cm enclosure for each probe.

Fig. 11 displays the calculated power of the signal in frequency ranges from 300 MHz to 3 GHz and from 300 MHz to 2 GHz for different enclosure diameters. The signal power calculated in an enclosure of 30 cm diameter is more than the values calculated in the enclosures of other diameters. The calculated values by each probe located inside an enclosure of 40 cm diameter is almost half of the one located inside an enclosure of 30 cm diameter. However, the calculated values of probes in enclosures of 50 cm and 60 cm diameter are almost the same.

Therefore, it can be concluded that by increasing the enclosure diameter to over 40 cm, the signal power in the frequency range from 300 MHz to 2 GHz remains unchanged, and the distance from the PD source has no significant effect on the sensitivity of the PD measurements. Meanwhile, there is a significant difference among the calculated power of the signal in different compartments in frequency ranges of 0.3-2 GHz and 0.3-3 GHz. As it can be seen in Fig. 11, the calculated power of the signal in each compartment in the frequency range of 0.3-2 GHz is almost half of the related calculated value in the frequency range of 0.3-3 GHz.

3.2. Effects of GIS Spacer

The presence of a spacer within the structure of a GIS and its effect on PD-based EM wave propagation can be studied from two points of view. In one study, the spacer thicknesses, and in the second, the type of the spacer is investigated. Different manufacturers may employ different spacer thicknesses under different operating voltage levels. To analyze the impacts of gas barrier spacer thickness, the spacer with thicknesses of 2 cm, 3 cm, 4 cm, and 5 cm are investigated. The simulation results show no significant differences between the peaks of the electric field calculated using the different probes. Fig. 12 displays the power of the signal in the frequency ranges of 300 MHz to 3 GHz and 300MHz to 2 GHz. The magnitude of wave presented in this

figure is in per-unit with reference to the 'probe C' of compartment 1, which calculated magnitude of 2 cm spacer thickness. The signal power calculated by probes, located in different compartments probe, is increased slightly as a function of the spacer thickness increment change. However, the spacer thickness affects the PD-based EM wave propagation negligibly in the frequency range of 0.3-2 GHz.

There are two types of spacers within the GIS structure: the gas barrier and the support insulator. With a gas barrier, the gas inside the two adjacent compartments cannot flow through the barrier. However, when a support insulator is employed, the gas between the two adjacent compartments can move through this insulator (Fig. 13).

A support insulator usually has three or four holes in its structure. Fig. 14 presents the signal power of PD-based EM wave propagation when different types of spacers are used. As can be seen, the signal power of UHF probes in the frequency range of 0.3-3 GHz is almost 60 percent of the power of an identical probe in the frequency range of 0.3-2 GHz. Also, in the frequency range of 0.3-3 GHz, the signal power of probe 5 is more than that of probe 4. This is due to reflections of PD-based EM waves at the end of the structure model.

However, in the frequency range of 0.3-2 GHz, the signal power decreases as one gets far away from the PD source, and the difference between the three types of the spacer is negligible. This means that the reflected wave from the end of the straight model has more components in the frequency range of 2-3 GHz. Finally, it can be concluded that each probe in the straight structure of GIS with different spacer types can cover at least 5 m for both PD localization and pattern recognition purposes.

3.3. Effects of Disconnector

As is shown in Fig. 4, a disconnector is considered at compartment 2 of the straight GIS model. The electric fields calculated by probes 1 to 5 are shown in Fig. 15. The distance between contacts of the conductor is varied from 10 to 30 cm. The first peak of the electric field is in per-unit of 'probe 1-C' peak. By increasing the contact distance of the disconnector, the decrement of the electric field peak will rise. In Fig. 16, the signal power in the frequency range of 0.3-2 GHz is almost the same for different contact distances of the disconnector. As a result, although the disconnect gap has no significant effects on PD-based EM wave signal power, it can result in a considerable reduction in the first peak of the calculated electric field. Since the PD localization within GIS is based on the time arrival difference of first electric field peaks to different sensors, this can result in errors in the estimation of the PD source position. Therefore, it is better to apply PD sensors beside each disconnector's contacts in a GIS arrangement to ensure high accuracy in analyzing the results.

3.4. Effects of L-Shape Structure

The L-Shape structure used in this study is shown in Fig. 5. In each compartment, except for compartment 3, one set of electric field probes is located in the middle of the compartment. The positions of these electric field probes around the periphery are in direction angles of 0, 180, and 90 degrees with respect to the PD source position. In compartment 3, two sets of electric field probes are located, one in the straight part of PD occurrence (probe 3) and the other farther after the L-shape structure (probe 4). The calculated first peak of the electric field is shown in Fig. 17. The calculated electric field peak of probe 4, in comparison to the probe 3 measurement, is significantly lower. Fig. 18 depicts the power of the signal calculated in the frequency ranges of 0.3-2 GHz and 0.3- 3GHz.

The signal power in the frequency range of 0.3-2 GHz decreases with a steady gradientgradient. However, the signal power decrement rate, when the probe is relatively far from the PD source (i.e., in probe 4), is much higher than this decrement rate for the other probes.

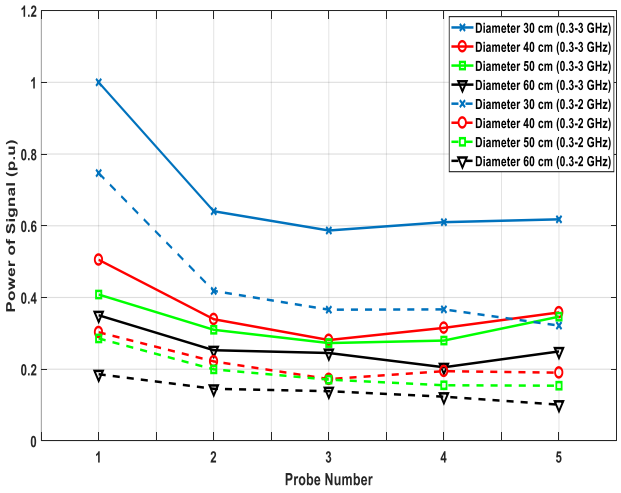

Fig. 11: The effects of different enclosure diameters on signal power in the frequency ranges of 0.3-2 GHz and 0.3-3 GHz.

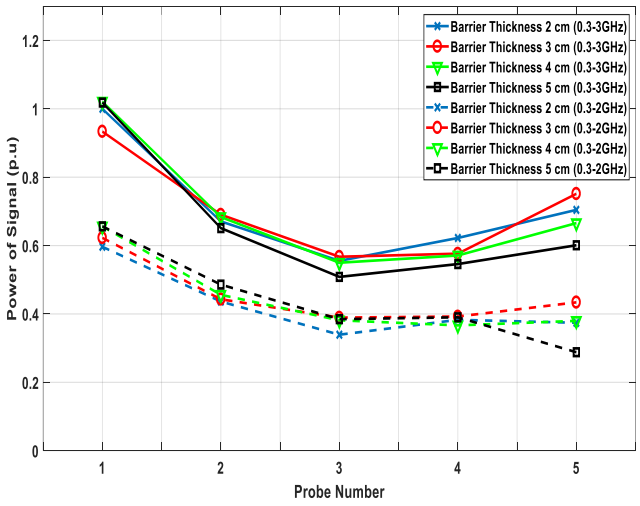

Fig. 12: The effects of barrier thickness on signal's power in the frequency range of 0.3-2 GHz and 0.3-3 GHz.

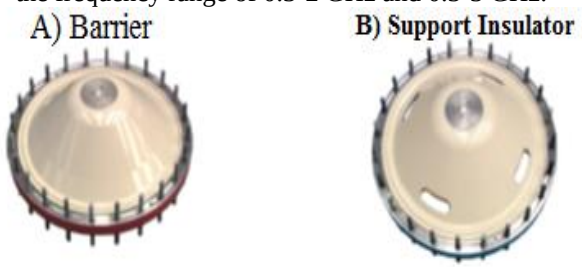

Fig. 13: Two types of spacers including (a) gas barrier, and (b) support insulator.

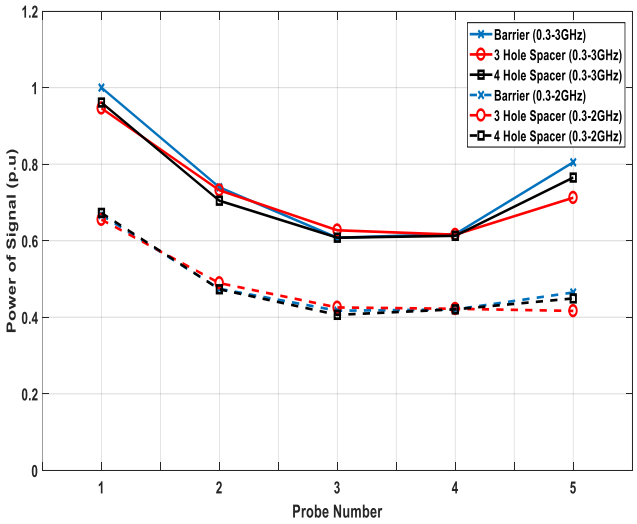

Fig. 14: The effects of spacer types on signal power in the frequency ranges of 0.3-2 GHz and 0.3-3 GHz.

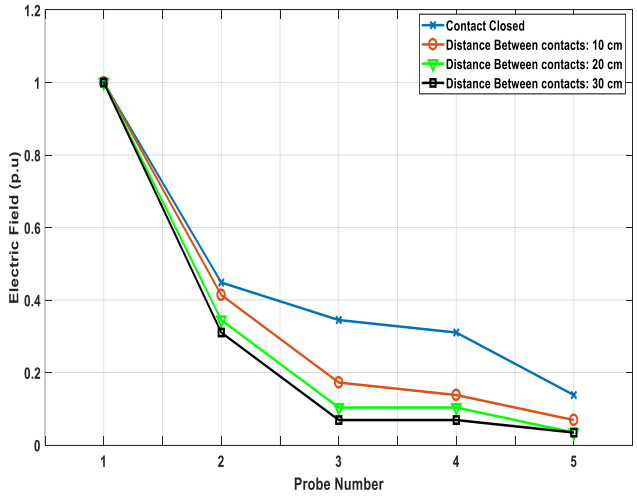

Fig. 15: The effects of disconnector contact distance on the first peak of the calculated electric field.

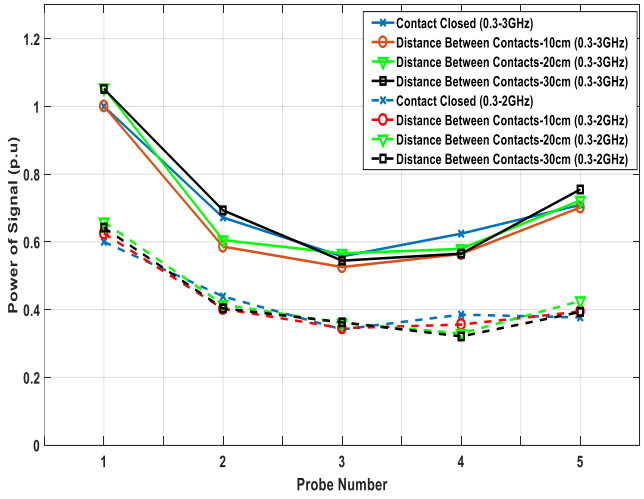

Fig. 16: The effects of disconnector contact distance on signal power in the frequency ranges of 0.3-2 GHz and 0.3-3 GHz.

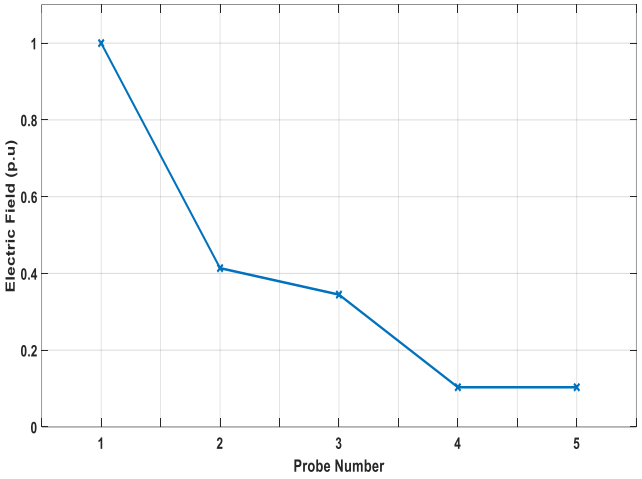

Fig. 17: The effects of L-shape structure on the first peak of the calculated electric field.

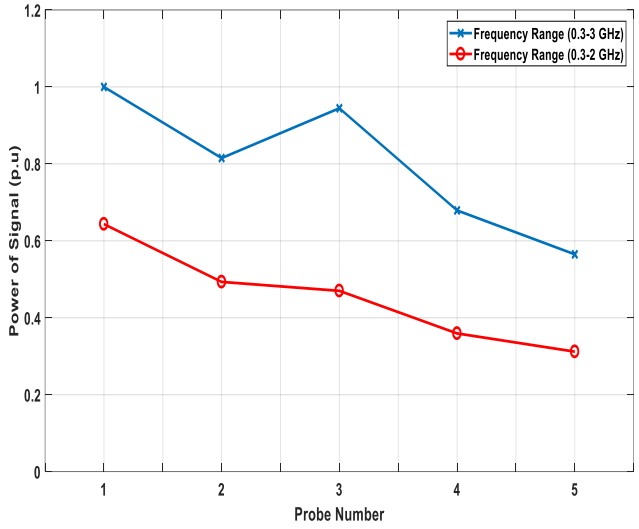

Fig. 18: The effects of L-shape structure on signal power in the frequency ranges of 0.3-2 GHz and 0.3-3 GHz.

Therefore, it can be concluded that the high-frequency components of the signal cannot pass through the L-shape structure section of the GIS. However, the decrement of the signal's power in a frequency range of 0.3-3 GHz is not related to the L-Shape structure, and it is the result of getting far from the PD source. As a result, although the signal power in these frequency ranges is almost steady for different probes in the L-shape structure, the calculated first peak of the electric field experiences a significant reduction after passing through L-shape part of the structure. This can have some effects on analyzing the calculated results, especially when PD is localized. Hence, it is better to have PD sensors in both L-shaped sections of the GIS structure.

3.5. Effects of T-Shape Structure

Fig. 6 shows the T-shape structure, which is employed to study PD-based EM wave propagation. In each compartment, except for compartment 3, one set of electric field measuring probes are applied just in the middle of the compartment. The position of the electric field probes is in direction angles 0, 180, and 90 degrees based on the PD source position. In compartment 3, like the L-shape structure, two sets of electric field probes are considered – one set in a straight direction

(probe 3) and the other in the T-branch indirect line (probe 6) with PD source. The probes marked number 7 are placed in compartment 6. In Fig. 19, the first peak of the electric field calculated on the capture of the PD-based EM wave is shown. By comparing the results of probes 4 and 6, the decrement of the signal peak in the T-branch section is shown to be more than that in the straight section. As a function of the distance increment of the UHF probe from the PD source position, the electric field peak is decreased. Fig. 20 shows the variations of power of the signal in the frequency ranges of 0.3-2 GHz and 0.3-3 GHz. As can be seen, the PD-based EM waves after passing through the T-branch section of the structure lose the high and low frequency of their powers. However, the power decrement in the frequency range of 0.3-3 GHz is more than the power decrement in the frequency range of 0.3-2 GHz. The reason is that when the PD-based EM waves are crossing a GIS T-structure, only the TEM mode of those signals will pass through while most of the TE mode of signals will be lost. As can be seen, the power of the signal in probe 7 is less than half of the power calculated by probe 1 in the frequency range of 0.3-2 GHz. Therefore,

when passing through the T-branch GIS structure, PD EM waves can lose both their signal power and their calculated first electric field. However, in the straight branch of the T-shape structure, there are no significant changes in the signal power, while a 50% decrement is seen in the first peak of the calculated electric field. Accordingly, for both PD localization and distinguishing defect type purposes, a PD sensor should be located in the T-branch of the GIS structure.

4. Summary And Conclusion

The GIS busbar components and structure have impacts on the calculated values of PD EM waves and the signals captured by UHF sensors. Accordingly, this paper examines the impact of the position and direction angle of PD sensors versus different PD sources on the calculated signals. It is shown that the PD sensors having a direction angle of 90 degrees versus the PD source have the lowest sensitivity regarding the PD signal measurements. Also, the following five conclusions have been investigated and verified:

1- It is shown using the calculation results that as the enclosure diameter is increased, the size of the first peak of the PD signal (electric field) is reduced. However, the signal power in the frequency range of 0.3-2 GHz encounters a small change when the enclosure diameter is increased.

2- It is also shown using the calculation results that the spacer thickness has a small impact on the size of the first peak of the electric field and the signal power in the frequency range of 0.3-2 GHz. Also, it is shown that the spacer type (i.e. a gas barrier or support insulator with three or four holes) has small effects on the EM-related PD calculated signal. Therefore, each probe in the straight structure section of GIS (with different spacer types) can cover at least a distance of 5 m for both PD localization and pattern recognition purposes.

3- The variations in the size of a disconnector gap distance (at different operating voltage levels of a GIS) affect the PD-based EM wave propagation process. As its contacts gap increases, the size of the first peak in its electric field reduces. However, the signal power in the frequency range of 0.3-2 GHz is much less influenced by contact gap distances. Hence, for PD localization purposes, it is better to apply a PD sensor after each disconnector contact in the GIS arrangements.

4- The L-shape structure of GIS can result in a significant reduction in the calculated first peak of the PD signal electric field. However, the reduction in the gradient of its signal power in the frequency range of 0.3-3 GHz is increased while the gradient of power decrease in the frequency range of 0.3-2 GHz is constant. This means that the high-frequency TE modes of a signal cannot pass through the L-shape structure. Therefore, it is better to locate PD sensors on both sides of a GIS L-shape structure to identify the PD defects type and to localize the PD source.

5- A GIS busbar of the T-shape structure attenuates the EM PD wave propagation. The PD signal's first peak, when passed through a T-branch structure, is compared against the signal's peak in a straight branch. It is shown that in the former case, the signal is significantly reduced. Additionally, the signal's power reduction gradient in a T-branch is more than the one (at the same compartment) in a straight branch. This reduction is about half of the signal power reduction when passing through a T-branch structure. Hence, it is essential to locate a PD sensor in the T-branch of a GIS structure to localize the PD source and to identify the type of PD.

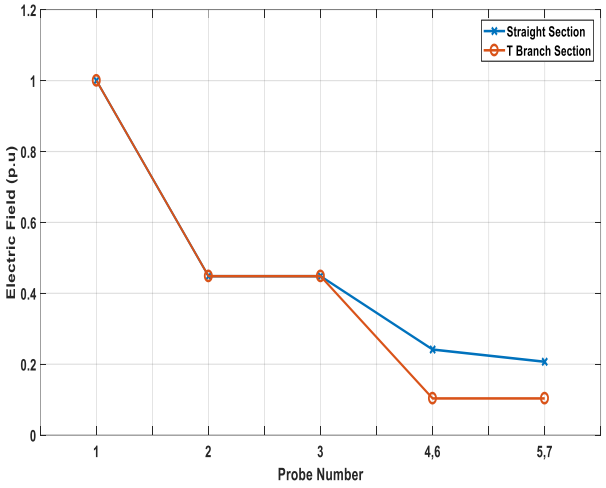

Fig. 19: The effects of T-shape structure on the first peak of the calculated electric field.

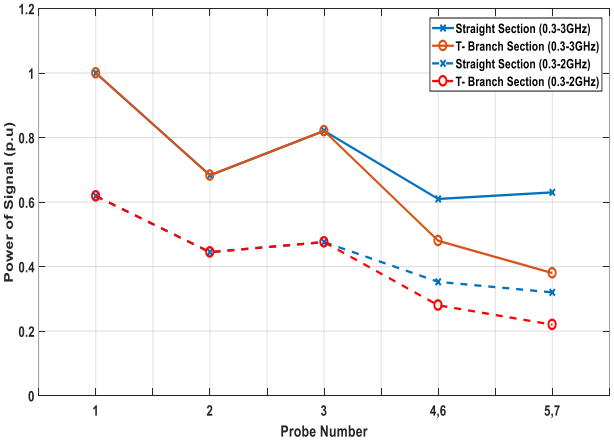

Fig. 20: The effects of T-shape structure on signal power in the frequency ranges of 0.3-2 GHz and 0.3-3 GHz.

CREDIT AUTHORSHIP CONTRIBUTION STATEMENT

Reza Rostaminia: Conceptualization, Data curation, Formal analysis, Investigation, Methodology, Project administration, Resources, Software, Supervision, Validation, Visualization, Roles/Writing - original draft, Writing - review & editing. **Mehdi Vakilian**: Investigation, Supervision, Validation, Visualization, Writing - review & editing. **Keyvan Firouzi**: Data curation, Supervision, Validation, Visualization, Writing - review & editing.

DECLARATION OF COMPETING INTEREST

The authors declare that they have no known competing financial interests or personal relationships that could have appeared to influence the work reported in this paper. The ethical issues; including plagiarism, informed consent, misconduct, data fabrication and/or falsification, double publication and/or submission, redundancy has been completely observed by the authors.

REFERENCES

[1] X. Li, X. Wang, D. Xie, X. Wang, A. Yang, and M. Rong, "Time–frequency analysis of PD-induced UHF signal in GIS and feature extraction using invariant moments," *IET Science, Measurement & Technology*, vol.12, no. 2, pp. 169-175, 2018.

[2] F. Bin, F. Wang, Q. Sun, S. Lin,Y. Xie, and M. Fan, "Internal UHF antenna for partial discharge detection in GIS," *IET Microwaves, Antennas & Propagation*, vol. 12, no. 14, pp. 2184-2190, 2018.

[3] X. Li, X. Wang, A. Yang, M. Rong, "Partial discharge source localization in GIS based on image edge detection and support vector machine," *IEEE Transactions on Power Delivery*, vol. 34, no. 4, pp. 1795-1802, 2019.

[4] C. Zachariades, R. Shuttleworth, R. Giussani, and T. Loh, "A Wideband spiral UHF coupler with tuning nodules for partial discharge detection," *IEEE Transactions on Power Delivery*, vol. 34, no. 4, pp. 1300-1308, 2019.

[5] CIGRE, *UHF Partial Discharge Detection System for GIS: Application Guide for Sensitivity Verification*, pp. 1-35, 1995.

[6] K. Firuzi, M. Vakilian, B. T. Phung and T. R. Blackburn, "A hybrid transformer PD monitoring method using simultaneous IEC 60270 and RF data," *IEEE Transactions on Power Delivery*, vol. 34, no. 4, pp. 1374 - 1382, 2019.

[7] H. Muto, M. Doi, H. Fujii, and M. Kamei, "Resonance characteristics and identification of modes of electromagnetic waves excited by partial discharges in GIS," Electrical *Engineering in Japan*, vol. 131, no. 2, pp. 1-11, 2000.

[8] M. Shi, X. Han, X. Zhang, Z. Zhang, and J. Li, "Effect of disconnector and high-voltage conductor on propagation characteristics of PD-induced UHF signals," *IET High Volt*, vol. 3, no. 3, pp. 187-192, 2018.

[9] S. Okabe *et al*, "Simulation of propagation characteristics of higher order mode electromagnetic waves in GIS," *IEEE Transactions on Dielectrics and Electrical Insulation*, vol. 13, pp. 855-861, 2006.

[10] M. Yoshimura, H. Muto, C. Nishida, M. Kamei, S. Okabe, and S. Kaneko, "Propagation properties of electromagnetic wave through T-branch and obliquely angled tank," *IEEE Transactions on Dielectrics and Electrical Insulation*, vol. 14, pp. 328-333, 2007.

[11] S. Okabe, S. Kaneko, M. Yoshimura, H. Muto, C. Nishida, and M. Kamei, "Partial discharge diagnosis method using electromagnetic wave mode transformation in gas insulated switchgear," *IEEE Transactions on Dielectrics and Electrical Insulation*, vol. 14, no. 3, pp. 702-709, 2007.

[12] S. Kaneko, S. Okabe, M. Yoshimura, H. Muto, C. Nishida, and M. Kamei, "Partial discharge diagnosis method using electromagnetic wave mode transformation in actual GIS structure," *IEEE Transactions on Dielectrics and Electrical Insulation*, vol. 15, no. 5, pp. 1329-1339, 2008.

[13] M. Hikita, S. Ohtsuka, G. Ueta, S. Okabe, T. Hoshino, and S. Maruyama, "Influence of Insulating Spacer Type on Propagation Properties of PD-induced Electromagnetic Wave in GIS," *IEEE Transactions on Dielectrics and Electrical Insulation*, vol. 17, no. 5, pp. 1643-1648, 2010.

[14] T. Hoshino, Sh. Maruyama, and T. Sakakibara, "Simulation of propagating electromagnetic wave due to partial discharge in GIS using FDTD," *IEEE Transaction on Power Delivery*, vol. 24, no. 1, pp. 153-159, 2009.

[15] S. Kaneko, S. Okabe, H. Muto, M. Yoshimura, C. Nishida, and M. Kamei, "Electromagnetic wave radiated from an insulating spacer in gas insulated switchgear with partial discharge detection," *IEEE Transactions on Dielectrics and Electrical Insulation*, vol. 16, no. 1, pp. 60-68, 2009.

[16] M. Hikita, S. Ohtsuka, S. Okabe, J. Wada, T. Hoshino, and S. Maruyama, "Influence of disconnecting part on propagation properties of PD induced electromagnetic wave in model GIS," *IEEE Transactions on Dielectrics and Electrical Insulation*, vol. 17, no. 6, pp. 1731-1737, 2010.

[17] M. Hikita, S. Ohtsuka, T. Hoshino, S. Maruyama, G. Ueta and S. Okabe, "Propagation properties of PD-induced electromagnetic wave in GIS model tank with T branch structure," *IEEE Transactions on Dielectrics and Electrical Insulation*, vol. 18, no. 1, pp. 256-263, 2011.

[18] M. Hikita, S. Ohtsuka, J. Wada, S. Okabe, T. Hoshino, and S. Maruyama, "Propagation properties of PD-induced electromagnetic wave in 66 kV GIS model tank with L branch structure," *IEEE Transactions on Dielectrics and Electrical Insulation*, vol. 18, no. 5, pp. 1678-1685, 2011.

[19] H. Koch, *Gas-insulated transmission lines*. John Wiley & Sons, 2012.

BIOGRAPHY

Reza Rostaminia received the B.Sc. degree in Electrical and Electronics Engineering from Babol Noshirvani University of Technology, Babol, Iran in 2007, The M.Sc. degree in Electrical Power Engineering from Khaje Nasir Toosi University of Technology (KNTU), Tehran, Iran in 2011 and the Ph.D. degree in Electric Power Engineering (High Voltage Engineering) from Shahid Chamran University of Ahwaz, Ahwaz, Iran in 2017. He was a post-doctoral researcher at the same university from 2019 to 2020. From 2015 to 2018, he was a sabbatical study in Electric Power Engineering (High Voltage Engineering) from Sharif University of Technology, Tehran, Iran in 2021. He joined the Parsian Substation Development Company, Tehran, Iran, where he is currently Technical Head of HV Substation Equipment Department. His research interest is High Voltage Engineering, Dielectrics and Insulation, Partial Discharge, Condition Monitoring and Diagnosis of High Voltage Equipment, High Voltage Substation Design and Earthing design.

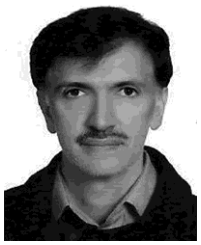

Mehdi Vakilian (M'88–SM'15) received the B.Sc. degree in electrical engineering and the M.Sc. degree in electric power engineering from the Sharif University of Technology, Tehran, Iran, in 1978 and 1986, respectively, and the Ph.D. degree in electric power engineering from Rensselaer Polytechnic Institute, Troy, NY, USA, in 1993. From 1981 to 1983, he was with Iran Generation and Transmission Company, and then with the Iranian Ministry of Energy from 1984 to 1985. Since 1986, he has been with the Faculty of the Department of Electrical Engineering, Sharif University of Technology. During 2001–2003, and 2014-2018 he was the Chairman of the department. During 2003 to 2004, and part of 2007, he was on leave of study at the School of Electrical Engineering and Telecommunications, University of New South Wales, Sydney, Australia. His research interests include transient modeling of power system equipment, especially power transformers, optimum design of high-voltage equipment insulation, monitoring of power system equipment and their insulations, especially with partial discharge measurement, power system transients, and distribution system studies.

Keyvan Firuzi received the B.Sc. degree in Electrical and Electronics Engineering from University of Tabriz, Tabriz, Iran in 2012, The M.Sc. degree in Electrical Power Engineering and the Ph.D. degree in Electric Power Engineering (High Voltage Engineering) from Sharif University of Technology, Tehran, Iran in 2014 and 2019 respectively. He was a post-doctoral researcher at the same university from 2019 to 2020. From 2015 to 2018, he was a Research Scientist with Niroo Research Institution (NRI). In 2021, he joined the Electrical and Electronics Engineering Department at METU, where he is currently working as an Assistant Professor. His research interest is High Voltage Engineering, Dielectrics and Insulation, Partial Discharge, Condition Monitoring and Diagnosis of High Voltage Equipment, Signal Processing, and Machine Learning.